Use of micro-computed tomography imaging and porosity measurements as indicators of collagen preservation in archaeological bone

Jennifer A. Tripp[1,*], Maria E. Squire[2], Robert E. M. Hedges[3], Rhiannon E. Stevens[1]

[1] UCL Institute of Archaeology, London, UK

[2] Department of Biology, University of Scranton, PA, USA

[3] Research Laboratory for Archaeology, University of Oxford, UK

* corresponding author: j.tripp@ucl.ac.uk

Institute of Archaeology

University College London

31-34 Gordon Square

King's Cross

London WC1H 0PY

United Kingdom

ABSTRACT

Collagen isolated from archaeological bone is a common material for radiocarbon dating, stable isotope analysis, and zooarchaeology by mass spectrometry (ZooMS). However, not all bones contain extant collagen, leading to unnecessary destruction of unproductive bones and wasted laboratory time and resources. An aim of this research is to study bone diagenesis, particularly collagen destruction, in an effort to develop a minimally destructive method for identifying bones with high collagen content. In a multi-method study of variably preserved bones from Etton, Cambridgeshire, UK, we examined material properties of Neolithic cattle and sheep bones including porosity, surface area, and elemental composition. Micro-computed tomography (microCT) is an imaging technique that furnishes three-dimensional images of mineralized materials such as bone. Cortical bone porosity, the percentage of total bone volume consisting of empty space as calculated using microCT, can act as a proxy for bone collagen preservation. In general, bones with high cortical porosity are unlikely to contain sufficient collagen for further analysis. Bones with apparently low cortical porosity have a more varied range of collagen preservation. Bone samples with low porosity and no extant collagen often contain micropores with a diameter of 10 nm or less that cannot be seen in microCT images but are apparent in pore size distributions measured by mercury porosimetry, and indicated by high surface areas measured by nitrogen adsorption. Furthermore, a re-evaluation of light-induced breakdown spectroscopy data from this same assemblage confirms that ratios of calcium to fluorine may likewise indicate the state of diagenesis.

KEYWORDS: micro-computed tomography; light-induced breakdown spectroscopy; BET nitrogen adsorption; mercury porosimetry; bone diagenesis; cortical porosity; bone collagen; radiocarbon dating; stable isotope analysis

1. INTRODUCTION

Collagen isolated from archaeological bone is a commonly-used material for radiocarbon dating, stable isotope analysis, and zooarchaeology by mass spectrometry (ZooMS). Much discussion exists in the literature about the exact composition of this substance called "collagen" that comes from archaeological bones (DeNiro & Weiner 1988). Collagen from fresh bones is a well-defined triple-helical protein, but that from ancient bones, while resembling modern collagen, has significant physical differences that develop over time. Ancient bone collagen is susceptible to both degradation (breakage of bonds and the removal of endogenous material) and contamination (the introduction of exogenous material) which can render its use for further analysis problematic (van Klinken 1999).

Numerous collagen extraction protocols have been developed, which generally involve demineralization, followed by gelatinization to solubilize the collagen; these procedures also sometimes include further steps such as a solvent wash, base wash, or ultrafiltration (Cleland, et al. 2012; Brock, et al. 2013; Sealy, et al. 2014; Cersoy, et al. 2017; Brock, et al. 2018). Quality of the collagen is evaluated using C:N ratios (van Klinken 1999). Generally, these protocols are time-consuming, and all too often the lengthy procedures result in little or no yield of collagen that can be used for further analysis. Because not all bones contain extant collagen, unnecessary destruction of unproductive bones and wasted laboratory time and resources are the result when sampling and pretreatment is initiated on unsuitable bones. Unfortunately, visual inspection of bones does not offer a useful indication of collagen preservation, so other methods to study bone preservation must be developed.

Chemical isolation of collagen from archaeological bone is both necessitated and complicated by degradation of collagen due to diagenesis, and much effort has gone into trying to understand the post-mortem taphonomic changes that occur in bone, from both forensic and archaeological perspectives (Behrensmeyer & Kidwell, 1985). Much has been

written about the specific mechanisms of bone diagenesis, and it's generally agreed that decay is due to two routes: microbial attack and physicochemical processes, both of which can change bone histology and be observed using microscopy. Jackes, et al. (2001) describe the bacterial action as leaving channels of just under 1 μm within the bone, as observed by scanning electron microscopy (SEM). They note that bacterial action lowers the pH within the bone, leading to mineral dissolution and re-precipitation that causes an increase in crystallinity. Bacterial action in their experiments doesn't seem to affect collagen content, C:N ratios or C and N isotopic values, but this observation has been contradicted by others. In particular, Hedges (2002) describes microbial attack as the primary mechanism for collagen loss, although in warmer climates physicochemical processes also play a significant role. In addition to bacterial attack, fungal action can lead to Wedl tunneling, characterized by pores 5-10 μm in diameter (Marchiafava, et al. 1974; Trueman & Martill 2002; Jans, et al. 2004). Microbial decay can begin hours after death (Bell, et al. 1996), and is more pronounced in whole burials rather than defleshed or dismembered bones, due to the action of gut bacteria (Trueman & Martill 2002).

Smith, et al. (2007) measured ten diagenetic parameters on nearly 200 bones from Holocene Europe, and identified four diagenetic states: (1) well-preserved bones, which have high % collagen and low porosity; (2) bones showing accelerated collagen hydrolysis, which demonstrate good histological preservation but low % collagen; (3) microbially-attacked bones, which show increased porosity due to tunneling and lower % collagen; and (4) bones with catastrophic mineral dissolution, which have low % collagen and an increase in large pores leading to reduced density. They suggest that the diagenetic trajectory of a given bone correlates more strongly with early taphonomic history, such as whether the bone was defleshed or cooked, rather than with soil conditions, so that the state of preservation of a given bone isn't necessarily site-specific.

However, site hydrology can affect the preservation of bone mineral and collagen (Hedges & Millard 1995; Nielsen-Marsh & Hedges 2000; Gutierrez 2001). Additionally, collagen loss is accelerated at sites with high temperatures (Collins, et al. 1995; Smith, et al. 2002). Hedges, et al. (1995), however, also note that it is possible for bone to retain good histological structure but still lose its collagen, by an unknown mechanism. Collagen is best preserved when it is closely associated with bone mineral (Child 1995; Collins, et al. 2002). Lees (1989) notes that mineralized collagen is not susceptible to collagenase degradation and also requires a higher temperature for denaturation compared to non-mineralized collagen. Thus, processes that lead to demineralization will also promote collagen loss.

Because bone preservation is so variable, and bone pretreatment protocols are destructive and time-consuming, numerous studies have attempted to find quick, minimally destructive prescreening methods to assess collagen content before destructive sampling and laboratory purification commence. The most common method uses % nitrogen or C:N ratio of whole bone (Ambrose 1990; Bocherens, et al. 2005; Brock, et al. 2012; Jacob, et al. 2018). In general, authors report that low %N and variable C:N ratios can indicate poor collagen preservation. However, recent work (Jacob, et al. 2018) found that intrabone %N can be quite variable and that bones with marginal %N can still yield enough collagen for stable isotope analysis or radiocarbon dating, making this currently routine prescreening metric a less certain indicator of bone collagen preservation. Examination of bone histology using optical microscopy (Hackett 1981; Yoshino, et al. 1991; Hedges, et al. 1995; Trueman & Martill 2002; Hollund, et al. 2012; Huisman, et al. 2017) or various SEM techniques (Turner-Walker & Syversen 2002; Jans, et al. 2002; Reiche, et al. 2003; Huisman, et al. 2017) can show qualitative diagenetic changes, but quantitative screening is hindered by differences in image interpretation by different users. Spectroscopic methods such as Fourier-transform infrared spectroscopy (FTIR) or FT-Raman have been extensively used to study bone crystallinity by

using carbonate peak intensities to calculate the infrared splitting factor (IRSF) (Wright & Schwarcz 1996; Surovell & Stiner 2001; Reiche, et al. 2003; Morris & Finney 2004; Trueman, et al. 2008; Stathopoulou, et al. 2008; Chadefaux, et al. 2009; Brock, et al. 2010; King, et al. 2011; Hollund, et al. 2013; Halcrow, et al. 2014; Lebon, et al. 2014; Pestle, et al. 2014; France, et al. 2014; Pestle, et al. 2015; Lebon, et al. 2016). The introduction of hand-held FTIR and Raman instruments hold promise for screening bones in the field and in museums; however, IRSF values do not always correlate with collagen preservation. The identification of peaks specific to collagen, such as the amide I peak at 1636 cm^{-1}, hold more promise but are more difficult to detect using the portable hand-held instruments (Chadefaux, et al. 2009; France, et al. 2014; Lebon, et al. 2016; Madden, et al. 2018). Other methods for predicting collagen preservation, such as trace element analysis (King, et al. 2011; Fernandes, et al. 2013), laser-induced breakdown spectroscopy (Rusak, et al. 2011), X-ray and neutron radiography (Sołtysiak, et al, 2018), tensile strength (Turner-Walker & Parry 1995), and differential scanning calorimetry (Nielsen-Marsh, et al. 2000) have met with mixed success. Presumably, the different possible diagenetic states lead to non-uniform analytical results, making for irregular correlation with collagen preservation.

Some of the most promising potential methods for studying bone diagenesis and predicting collagen preservation are those which measure the surface area or porosity of bone. Biological action or physical dissolution of the bone leads to measurable changes in bone porosity, typically with a decrease in the number of micropores and an increase in macropores, and an overall loss of bone density (Hedges, et al. 1995). We will follow the definition of pore size ranges given by Turner-Walker, et al. (2002) and outlined in Table 1.

Over the last seventy years, various measurements of the surface area of bone have been carried out using the method of BET N_2 adsorption (Brunauer, et al. 1938). Wood (1947) first measured the surface area of bone apatite, and also found that tooth dentine and

enamel have significantly smaller surface areas than bone. Others since then have measured the surface area of fresh and decayed bone using the same method (Dry & Beebe 1960; Holmes, et al. 1964; Holmes, et al. 1970; Misra, et al. 1978; Weiner & Price 1986; reviewed by Lowenstein & Weiner 1989). Typical surface areas for bone are in the range of 80-120 m^2/g, but depend significantly on species, bone element, and experimental parameters such as the time and temperature of the degassing process, and ambient humidity.

The limitation of the BET method is that, while it can provide useful information about surface area and very small pores, it does not accurately measure the volume or diameter of larger pores. The upper limit for calculating pore size using gas adsorption is approximately 500 nm (Lowell, et al. 2004, p. 209). Consequently, mercury intrusion porosimetry (HgIP), which provides more accurate measurements of large pores (or, more accurately, pore entrance diameter) of over 200 μm diameter (Lowell, et al. 2004, p. 209; Giesche 2006), has also been used to study porosity changes with bone diagenesis. Holmes, et al. (1964) were the first to measure porosity of fresh bone using HgIP. Nielsen-Marsh & Hedges (1999) found a good correlation between protein content of archaeological bone, IRSF, and the microporosity of bone. An increased number of micropores (especially in the range of 4-10 nm) is observed in deproteinated bone. Turner-Walker, et al. (2002) further suggested that HgIP would be a useful tool for screening specimens not just for collagen but also for aDNA. Further studies demonstrated the utility of HgIP for studying diagenetic trajectories of bones from a variety of burial environments, and suggested correlation between low collagen content and high meso- and macroporosity (in the range of 0.1-8.5 μm) in their study of several hundred samples (Nielsen-Marsh, et al. 2007; Smith, et al. 2007). However, Brock, et al. (2010), in a much smaller study, did not see the same correlation between % collagen and HgIP bulk porosity.

While HgIP is useful for studying bone structure and predicting bone preservation, its utility as a prescreening method is limited by two factors: it is destructive, and it requires a fairly large amount of sample, typically at least 0.5 g. It would be preferable to have a minimally destructive method that would be suitable for screening whole bones or bone fragments for their suitability for collagen analysis.

Thus, we set out to explore the use of micro-computed tomography (microCT) for prescreening bones for collagen preservation. MicroCT uses X-rays to produce detailed three-dimensional images of materials. In particular, the method has long been used for scanning bones (see, e.g. Feldkamp, et al. 1989), including in vivo scans of small animals. In previous work (Tripp, et al. 2010) we showed a correlation between cortical bone porosity, as measured by microCT, and collagen recovery. The sample size was small, just four bones, but the work showed enough promise that a larger study was carried out, in conjunction with other measurements of bone microstructure such as HgIP and BET N_2 adsorption.

In the years since our initial publication other groups have used microCT to study the microstructure and diagenesis of forensic and archaeological bone (Beck, et al. 2012; Dal Sasso, et al. 2014; Booth, et al. 2016; Le Garff, et al. 2017; Ngan-Tillard & Huisman 2017). Le Garff, et al. (2017) used immediate post-mortem forensic studies to show that bone volume fraction tends to decrease over time, but the data are irregular and other parameters showed inconsistent trends. Studies of archaeological bones showed that microCT imaging enables one to distinguish between microbial and other decay (Booth, et al. 2016), but the promise of the technique has not yet been fully realized. In this work, we illustrate the potential of microCT imaging for studying bone diagenesis and predicting collagen preservation.

2. EXPERIMENTAL METHODS

2.1 Samples

Nineteen sheep and cattle long bones from the Neolithic causewayed enclosure at Etton, located near Peterborough in Cambridgeshire, England, were used in this study. In all cases, cortical bone was imaged and analyzed. The site of Etton has variable bone preservation, with some excavated bones having very high collagen recovery, and others containing no collagen at all (Hamilton & Hedges 2011). Sample information for the nineteen bones used in our study is listed in Table 2.

2.2 Micro-computed Tomography

Etton bone samples were scanned at The University of Scranton using a MicroCT 80 scanning system (μCT80, Scanco Medical, Switzerland). All samples were scanned vertically in a cylindrical sample holder (60mm D x 85 mm H), at a voltage of 55kV and intensity of 45 μA, and a resolution of 60 μm (isotropic voxel size). The time required to complete a scan of a 48 mm specimen is 4 hours. Multiple bones can be scanned simultaneously as long as they all fit within the sample holder and are kept from touching. In our previous publication (Tripp et al. 2010), we compared images scanned at 60 μm resolution with higher resolution images scanned at 30 μm isotropic voxel size, and found that the lower resolution was sufficient for analysis. Thus, we have used lower resolution scans for the analysis of the bones described here.

Quantitative analysis of the images was undertaken in order to determine any correlations between microCT images and collagen content. Cortical bone porosity (Ct.Po) was analyzed on a 9 mm region of each bone specimen. The chosen volume of interest (VOI) was in close proximity to the area from which a sample was previously taken for extraction of collagen and stable isotope analysis. For each bone specimen, image analysis was performed as described in our previous work (Tripp, et al. 2010) using contour lines that

consisted of a series of cylinders drawn within the bone structure. In cases of particularly dirty, cracked or fragmented specimens such an analysis offers a quicker and easier method than drawing whole bone contours, and our previous work showed that the results were comparable, and possibly superior to, whole bone contours. A typical analysis of a bone using the cylindrical contour method takes approximately 1-2 hours. Note that the cost of microCT scanning and analysis varies widely between institutions, which typically charge an hourly rate ranging from $25 to over $200 for use of the instrument and analysis of the images. Collaboration with other microCT users is likely the best route for archaeologists who wish to explore the technique and don't have access to an instrument at their home institution.

Prior to evaluation, a Gaussian filter (sigma = 0.8 voxels) removed noise from the images and segmentation, which separated bone from background, was done at thresholds ranging from 250 to 600 (increments of 50). The VOI was evaluated by the Scanco software at each threshold, and the bone volume fraction (BV/TV, where BV is bone volume and TV is total volume) values were recorded. Ct.Po was calculated from equation (1) (Lloyd et al 2008).

$$\mathbf{Ct.Po = 1 - BV/TV} \qquad (1)$$

In our previous work (Tripp, et al. 2010) we found that a threshold of 500 offered the best resolution and distinction between bones of differing preservation, so that is the threshold we have used for three-dimensional reconstruction and Ct.Po values reported in this study.

Mercury intrusion porosimetry

Samples were submitted to Micromeritics Analytical Services, where measurements were performed on an Autopore IV 9500 instrument. Sample sizes ranged from approximately 0.5 g to 1.2 g, and were in the form of solid bone chunks. Pore size

distribution was calculated from differential pressure measurements with mercury intrusion, assuming cylindrical pores, as described by Webb (1993).

2.3 BET Nitrogen adsorption

Surface area measurements of bone samples were done at Lawrence Berkeley National Laboratory, in the Molecular Foundry facility, using their ASAP 2010 BET adsorption apparatus (Micromeritics Instrument Corp). Approximately 1 g of bone, in chunks, was heated to 80 °C under vacuum for 1 hour for degassing. Pressure differential measurements with nitrogen adsorption were used to calculate surface area according to the Brunauer-Emmett-Teller method (Brunauer, et al. 1938), using the supplied instrument software. A typical analysis of a bone sample took 24 hours, though this can vary widely based on the nature of the sample and the number of differential pressures used in the measurements, and can be significantly reduced if a smaller range of pore sizes is targeted.

2.4 Laser-induced breakdown spectroscopy

LIBS measurements were done at the University of Scranton using a Nd:YAG laser operating at 1064 nm. Centering the spectral window at 680 nm enabled simultaneous observation of the F I 685.6 and Ca I 671.8 emissions, with no interference. The experiment, including a schematic diagram, is described in detail by Rusak, et al. (2011).

3. RESULTS and DISCUSSION

3.1 Micro-computed Tomography Imaging

MicroCT images for five of the bones used in this study are shown in Figure 1. Clear differences in the appearance of the bones indicates differences in morphology. For the most part, bones with no preserved collagen, such as ET51, look more porous than well-preserved bones, such as ET12. Some of the bones, such as ET18 and ET60 appear to have a bright,

dense, mineralized ring around the outside. Others, such as ET12 and ET62, contain large cracks.

More instructive than the simple flat images in Figure 1 are contour surfaces calculated by the microCT imaging software. A selection of these images is shown in Figure 2, and images for all of the bones used in this study are available in the supplemental information. Prior to the 3-D analysis, we select a threshold for differentiating between bone and non-bone within the analyzed volume. In line with our previous work (Tripp, et al. 2010) we have chosen to use a threshold of 500. It is clear at this threshold that, while several of the bones seem solid, others look very porous or indeed hollow within the portion of the shaft that was scanned. An extreme version of this is ET51, which shows the presence of dense material along the outer surface of the bone and lining the medullary cavity, but appears to lack mineralization between the two surfaces. Note that this does not mean that the space is actually empty, but just that the scanned density of the material is below the set threshold used when making the image.

3.2 microCT image analysis

Based on our previous work, we anticipated that we could use cortical porosity (Ct.Po), the percentage of total bone volume consisting of non-bone as calculated using microCT, as a proxy for bone collagen preservation. Values for Ct.Po for all of the bones are given in Table 2, and results are shown graphically in Figure 3, correlated with collagen preservation. From the graph two things become readily apparent. First, with one exception, all of the bones that have useful collagen recovery (>1% by mass of recovered collagen) have Ct.Po below 0.31. This makes sense given our discussion of bone diagenesis and the increased porosity that normally accompanies collagen decay. The exception is ET12, which has 5.7% collagen recovery, and also a very high Ct.Po. Examination of the microCT image from this bone shows a network of cracks, which serve to increase the calculated porosity

without necessarily leading to or resulting from collagen degradation. They may, for instance, be the result of physical impact during or after excavation. The second important aspect of the data is that bones with no collagen preservation have a wide range of Ct.Po values, from close to zero (implying no pores) up to nearly 0.8. This indicates that there may be several different mechanisms of collagen degradation within the site of Etton that result in different morphologies of the bone mineral. In practice, bones with high Ct.Po are unlikely to have significant collagen content, and can be excluded from analysis. Bones with low Ct.Po have a higher probability of collagen recovery, but may also contain no collagen. So, while microCT prescreening to eliminate bones with high Ct.Po may increase the likelihood of sampling bones that contain collagen, it is not a method that will enable complete removal of low-collagen bones from sampling.

3.3 Mercury intrusion porosimetry

In order to further understand how the Ct.Po values correlate with collagen recovery and other morphological parameters of the bone, a subset of four bones was analyzed using mercury intrusion porosimetry (HgIP). Total bulk porosity is the percent of total volume that consists of pores, and can be likened to Ct.Po. However, the actual values are different due to the different measurement methods. Total porosity measured by HgIP for four samples is given in Table 2. In general, for both measurements, the porosity increases with decreasing collagen preservation. However, HgIP bulk porosity seems to correlate more strongly with collagen preservation than Ct.Po. In particular, sample ET60 seems to have very low porosity as measured by microCT, but has quite high porosity measured by HgIP. This indicates that HgIP may be more sensitive to some pore size ranges than microCT.

A more useful way to view the HgIP data is using pore size distribution graphs. Nielsen-Marsh and Hedges (1999) previously published pore size distribution graphs for fresh modern bone, as well as for modern bone that was experimentally deproteinated using

hydrazine. The pore size distribution of modern bone, represented by the dark line in Figure 4, has a bimodal pore distribution, with a peak representing pores with diameter of approximately 10 μm, and another peak illustrating smaller pores just larger than 0.1 μm. The larger pores are thought to be the Haversian canals, which contain the blood vessels in bones, while the smaller are the canaliculi, small channels which connect the osteocyte-containing lacunae. These two pore sizes are also present in the deproteinated bone, but this bone additionally has a large number of very small pores, which are believed to be the spaces left behind when the collagen is removed.

The pore size distributions measured for four Etton sheep bones are shown in Figure 5, and the distributions show a number of interesting features. Note that the ET46, given by the dark solid line, appears remarkably similar to the fresh modern bone in Figure 4, with an additional small peak in the micropore region, indicating some loss of collagen. This bone has very good collagen preservation, with 13.4% recovered. At the other extreme is the poorly preserved ET51, represented by the gray solid line, which appeared very porous on the microCT images, and by HgIP has a significant number of pores in the mesopore to macropore range, with the distribution centered on 1 μm. This bone contains no collagen. The bone represented by the dashed line, ET62, contains 3.0% collagen, a low yield but still useful for radiocarbon dating or stable isotope analysis. The cortical porosity as measured by microCT is moderate and the bone appears porous, but the pore size distribution looks somewhat like the modern bone, with additional micropores and slightly elevated porosity in the macropore range. It is likely these macropores that are being detected in microCT, although their presence does not indicate complete collagen degradation. ET60 was a puzzling specimen, because it looks very well-preserved by microCT, with very low cortical porosity, but it has no preserved collagen. In the HgIP measurements it is apparent that the pore distribution of this bone (represented by the dotted line in Figure 5) looks almost

identical to the deproteinated modern bone measured by Nielsen-Marsh and Hedges (1999). The collagen has disappeared from this bone by some mechanism that has left the rest of the bone microstructure intact.

3.4 BET nitrogen adsorption

Six of the bones were further analyzed using BET nitrogen adsorption. Results of the BET surface area measurements for six bones are given in Table 2, and this same information is shown graphically in Figure 6. This chart shows surface area measurements for six bones (▲, left axis) correlated with collagen recovery. The four bones with the lowest collagen recovery have the highest surface areas, all measured to be over 100 m^2/g. Since surface area increases with increased porosity, particularly with the small pores that may form with collagen destruction, these results make sense. The better-preserved bones have lower surface areas, indicating better preservation; collagen is still present so microporosity is not elevated. Ct.Po from the bones is shown in the same figure (●, right axis). While the well-preserved bones clearly have low cortical porosity, as already discussed, the bones with no preserved collagen show variable cortical porosity. The results in this figure tell us two things. First, BET nitrogen adsorption seems to do a better job at identifying poorly preserved bones, most likely because it can detect much smaller pores than can be seen in microCT. An interesting case is that of ET60. This bone has a very low cortical porosity, possibly indicating good preservation by microCT, but it contains no collagen. The BET measurements reveal a very high surface area, indicating that the bone is quite porous, but that the pores are likely too small to be seen by microCT. We observed these micropores in the HgIP pore size distribution, and the BET adsorption data backs up the observation. Secondly, while low nitrogen adsorption surface area measurements may help with the identification of well-

preserved bones, it does not seem to do a good job at distinguishing between bones with no collagen and those with low, but still useful, collagen content.

3.5 Laser-induced breakdown spectroscopy

Rusak, et al. (2011) report LIBS data from thirteen of the Etton bones that we have imaged with microCT. LIBS instruments work by gradually ablating the surface of the bone with a laser and measuring the atomic ratios of the resulting vapor. In their analysis, Rusak, et al. found a positive correlation between collagen recovery and the measured Ca 671.8 / F 685.6 ratio of the bones. The average Ca/F ratio for ten pulses beginning with pulse 210 are given in Table 2 for the analyzed samples. In their publication, Rusak, et al. (2011) provide Ca/F ratios for all of the laser pulses, and a reanalysis of these results, plotted in Figure 7, is instructive. Figure 7 shows a significant difference of Ca/F ratios between bones that contain no collagen (black lines), and those with >1% collagen (light gray lines). At the surface of the bones, measured by the earlier laser pulses, there is little correlation between collagen content and Ca/F ratios. However, as the laser bores into the surface of the bones the Ca/F ratios of the two types of bones become resolved, with the collagen-containing bones having a higher Ca/F ratio. LIBS is a minimally destructive technique in that the laser does not bore deeply into the bone. After an analysis comprising approximately 220 laser pulses, the finished bone has a barely-visible channel with a crater depth on the order of 10^2 microns (Rusak et al. 2011).

Average values for the Ca/F ratios are plotted in Figure 8, and the difference between bones that contain collagen and those that do not is clear. Error bars represent 1 standard deviation on the average value for each set of bones. Clearly, bones with interior Ca/F ratios above about 5.5 tend to have usable collagen preservation levels, while those with Ca/F ratios lower than that have no collagen. It has been known for decades that fluorine concentration

increases in buried bones due to incorporation of fluoride ion into recrystallizing bone mineral (Parker, et al. 1974), and dating of buried bones by measuring fluorine content has been attempted (Kottler, et al. 2002). The fluorine diffusion profile in a bone varies based on its permeability as well as site-specific hydrology. Collagen preservation, too, depends on the interaction of the bone with its aqueous environment, so it makes sense that the fluorine concentration and collagen preservation may be correlated. However, it is difficult to draw conclusions based on results from a single site, so future work should measure variably preserved bones from other sites to see if the same trends are observed.

4. CONCLUSION

In general, bones with high Ct.Po as measured by microCT are unlikely to contain sufficient collagen for further analysis and can thus be excluded from a sampling assemblage. Bones with apparently low cortical porosity have a more varied range of collagen preservation. Bone samples with low Ct.Po and no recoverable collagen often contain micropores with a diameter of 10 nm or less that cannot be seen in microCT images but are apparent in pore size distributions measured by mercury porosimetry, and indicated by high surface areas measured by BET nitrogen adsorption. Such micropores are probably the space left behind by decaying collagen bundles.

Furthermore, a re-evaluation of LIBS data from this same assemblage confirms that ratios of calcium to fluorine may likewise indicate the state of diagenesis, with well-preserved bones measuring a lower Ca/F ratio than those with no extant collagen. However, fluoride content of archaeological bones is likely to be site-specific, and therefore future studies should be undertaken to see if the difference in Ca/F ratios observed in differentially preserved bones in Etton holds true at other sites, with samples of other ages, and in different environments. Thus, we conclude that cortical bone porosity as calculated by microCT can be used to exclude bones that are unlikely to contain collagen, while LIBS may provide further

information about their diagenetic state. Both methods hold promise as minimally destructive methods for bone prescreening, and future research should elucidate this further.

We have also shown that pore size measurements by HgIP and BET nitrogen adsorption are quite useful for studying bone diagenesis parameters and for predicting collagen preservation, but we should note here that neither method avoids destroying the bone samples in some manner. Both instruments require bone chunks or powder to be removed from the specimen for introduction into a small analysis chamber. HgIP is completely destructive, as the bone sample post-analysis is infused with mercury and must be disposed as toxic waste. For this reason, and the significant cost of analysis if an in-house instrument is not available, it is unlikely to become a routine pre-screening method despite its value for studying diagenetic trends. If the degassing temperature is not so high as to destroy the collagen within the bone, a sample used for BET nitrogen adsorption measurements should be able to be re-used for collagen extraction, but this has never been studied in a systematic way. LIBS can accommodate whole bones, depending on the size of the bone and the sample chamber, and results in a small surface abrasion. Thus, we have classified it as minimally destructive, and this technique along with microCT hold promise as pre-screening methods for collagen content of archaeological bones.

While microCT is often described as “nondestructive”, including in our earlier publication (Tripp, et al. 2010), more recent work has led to doubts about whether this is really true (Tuniz and Zanini 2014). Grün, et al. (2012) demonstrated that teeth subjected to microCT imaging subsequently gave erroneous ESR dates. Additionally, the field of radiation genetics has demonstrated for nearly a century that X-ray irradiation can lead to DNA damage (Muller 1927; Wolff 1971; Grosovsky, et al. 1998). Immel, et al. (2016) have found that exposure of archaeological bone samples to synchrotron radiation leads to significant loss of aDNA in ancient samples, but irradiation at levels normally seen in microCT did not

cause significant damage. This agrees with work by Paredes, et al. (2012), who found no damage to DNA in Hawaiian honeycreeper skins collected in the 1890s when irradiated at levels commensurate with microCT measurements. So, while microCT does not require cutting or drilling into a bone, and does not lead to significant visual changes in samples, underlying chemical degradation may result. However, the parameters leading to these changes are not well-established and until they are it seems prudent that samples to be imaged using microCT be carefully selected, and that non-imaged samples remain available to future researchers.

ACKNOWLEDGMENTS

The authors would like to thank Julie Hamilton of the University of Oxford for her assistance with the early work and for facilitating our use of the Etton bone samples, and Richard Sabin of the Natural History Museum in London for providing the samples. Jiri Urban (now at Masaryk University, Brno) and Sam Karenga (now at Mount Kenya University, Thika) assisted with the BET surface area measurements at Lawrence Berkeley National Laboratory. Chris Brown of Micromeritics, Inc. performed the mercury porosimetry measurements. Ryan Marisco and Dave Rusak of the University of Scranton did the LIBS measurements. JT and RES are funded by the European Research Council (Project 617777). MES recognizes the National Science Foundation (Award # 0722751) and the University of Scranton for funding. Lastly, we'd like to thank Fiona Brock, Hazel Reade, Sophy Charlton, and Tom Booth for helpful discussions about microCT and bone diagenesis.

REFERENCES

Ambrose, S.H., 1990. Preparation and Characterization of Bone and Tooth Collagen for Isotopic Analysis. J. Archaeol. Sci. 17, 431-451.

Beck, L., Cuif, J.-P., Pichon, L., Vaubaillon, S., Dambricourt Malassé, A., Abel, R.L., 2012. Checking collagen preservation in archaeological bone by non-destructive studies (Micro-CT and IBA). Nucl. Instr. Meth. Phys. Res. B 273, 203-207.

Behrensmeyer, A.K., Kidwell, S.M., 1985. Taphonomy's contributions to paleobiology. Paleobiol. 11, 105–119.

Bell, L.S., Skinner, M.F., Jones, S.J., 1996. The speed of post mortem change to the human skeleton and its taphonomic significance. Forensic Sci. Int. 82, 129-140.

Bocherens, H., Drucker, D., Billiou, D., Moussa, I., 2005. Une nouvelle approche pour évaluer l'état de conservation de l'os et du collagène pour les mesures isotopiques (datation au radiocarbone, isotopes stables du carbone et de l'azote). L'Anthropologie 109, 557–67.

Booth, T.J., Redfern, R.C., Gowland, R.L., 2016. Immaculate conceptions: Micro-CT analysis of diagenesis in Romano-British infant skeletons. J. Archaeol. Sci. 74, 124-134.

Brock, F., Dee, M., Hughes, A., Snoeck, C., Staff, R., Bronk Ramsey, C., 2018. Testing the effectiveness of protocols for removal of common conservation treatments for radiocarbon dating. Radiocarbon 60, 35-50.

Brock, F., Higham, T., Bronk Ramsey, C., 2010. Pre-screening techniques for identification of samples suitable for radiocarbon dating of poorly preserved bones. J. Archaeol. Sci. 37, 855-865.

Brock, F., Geoghegan, V., Thomas, B., Jurkschat, K., Higham, T.F.G., 2013. Analysis of bone "collagen" extraction products for radiocarbon dating. Radiocarbon 55, 445-463.

Brock, F., Wood, R., Higham, T.F.G., Ditchfield, P., Bayliss, A., Bronk Ramsey, C., 2012. Reliability of nitrogen content (%N) and carbon:nitrogen atomic ratios (C:N) as

indicators of collagen preservation suitable for radiocarbon dating. Radiocarbon 54, 879-886.

Brunauer, S., Emmett, P.H., Teller, E., 1938, Adsorption of Gases in Multimolecular Layers. J. Amer. Chem. Soc. 60, 309-319.

Cersoy, S., Zazzo, A., Lebon, M., Rofes, J., Zirah, S., 2017. Collagen extraction and stable isotope analysis of small vertebrate bones: A comparative approach. Radiocarbon 59, 678-694.

Chadefaux, C., Le Hô, A.-S., Bellot-Gurlet, L., Reiche, I., 2009. Curve-fitting micro-ATR-FTIR studies of the amide I and II bands of type I collagen in archaeological bone materials. E-PRESERVATIONScience 6, 129-137.

Child, A. M., 1995, Towards an understanding of the decomposition of bone in the archaeological environment, *Journal of Archaeological Science*, **22**, 165–74.

Cleland, T.P., Voegele, K., Schweitzer, M.H., 2012. Empirical evaluation of bone extraction protocols. PLoS One 7, 1-9.

Collins, M.J., Nielsen-Marsh, C.M., Hiller, J., Smith, C.I., Roberts, J.P., Prigodich, R.V., Wess, T.J., Csapo, J., Millard, A., Turner-Walker, G., 2002. The survival of organic matter in bone: a review. Archaeometry 44, 383-394.

Collins, M.J., Riley, M.S., Child, A.M., Turner-Walker, G., 1995. A Basic Mathematical Simulation of the Chemical Degradation of Ancient Collagen. J. Archaeol. Sci. 22, 175-183.

Dal Sasso, G., Maritan, L., Usai, D., Angelini, I., Artioli, G., 2014. Bone diagenesis at the micro-scale: Bone alteration patterns during multiple burial phases at Al Khiday (Khartoum, Sudan) between the Early Holocene and the II century AD. Palaeogeogr. Palaeoclimatol. Palaeoecol. 416, 30-42.

DeNiro, M.J., Weiner, S., 1988. Chemical, enzymatic and spectroscopic characterization of "collagen" and other organic fractions from prehistoric bones. Geochim. Cosmochim. Acta 52, 2197-2206.

Dry, M.E., Beebe, R.A., 1960. Adsorption studies on bone mineral and synthetic hydroxyapatite. J. Phys. Chem. 64, 1300-1304.

Feldkamp, L.A., Goldstein, S.A., Parfitt, G., Jesioil, G., Kleerkoper, M., 1989. The direct examination of three-dimensional bone architecture in vitro by computed tomography. J. Bone Min. Res. 4, 3-11.

Fernandes, R., Hüls, M., Nadeau, M.-J., Grootes, P.M., Garbe-Schönberg, C.-D., Hollund, H.I., Loynyk, A., Kienle, L., 2013. Assessing screening criteria for the radiocarbon dating of bone mineral. Nucl. Inst. Meth. Phys. Res. B 294, 226-232.

France, C.A.M., Thomas, D.B., Doney, C.R., Madden, O., 2014. FT-Raman spectroscopy as a method for screening collagen diagenesis in bone. J. Archaeol. Sci. 42, 346-355.

Giesche, H., 2006. Mercury Porosimetry: a General (Practical) Overview. Part. Part. Syst. Charact. 23, 1-11.

Grosovsky, A.J., de Boer, J.G., de Johg, P.J., Drobetsky, E.A., Glickman, B.W., 1988. Base substitutions, frameshifts, and small deletions constitute ionizing radiation-induced point mutations in mammalian cells. Proc. Nat. Acad. Sci. USA 85, 185-188.

Grün, R., Athreya, S., Raj, R., Patnaik, R., 2012. ESR response in tooth enamel to high-resolution CT scanning. Archaeol. Anthropol. Sci. 4, 25-28.

Gutierrez, M.A., 2001. Bone diagenesis and taphonomic history of the Paso Otero 1 Bone Bed, Pampas of Argentina. J. Archaeol. Sci. 28, 1277-1290.

Hackett, C.J., 1981. Microscopical focal destruction (tunnels) in exhumed human bones, Med. Sci. Law 21, 243–265.

Halcrow, S.E., Rooney, J., Beavan, N., Gordon, K.C., Tayles, N., Gray, A., 2014. Assessing Raman Spectroscopy as a Prescreening Tool for the Selection of Archaeological Bone for Stable Isotopic Analysis. PlosOne 9, e98462, 1-9.

Hamilton, J., Hedges, R.E.M., 2011. Carbon and nitrogen stable isotope values of animals and humans from causewayed enclosures. In: Whittle, A., Bayliss, A., Healy, F. (eds) Gathering Time: Dating the Early Neolithic Enclosures of Southern Britain and Ireland, Oxbow Books, Oxford, pp. 670-681.

Hedges R.E.M., 2002. Bone diagenesis: an overview of processes. Archaeometry 44, 319–328.

Hedges, R.E.M., Millard, A.R., 1995. Bones and Groundwater: Towards the Modelling of Diagenetic Processes. J. Archaeol. Sci. 22, 155-164.

Hedges, R.E.M., Millard, A.R., Pike, A.W.G., 1995. Measurements and relationships of diagenetic alteration of bone from three archaeological sites. J. Archaeol. Sci. 22, 201-209.

Hollund, H.I., Ariese, F., Fernandes, R., Jans, M.M.E., Kars, H., 2013. Testing an alternative high-throughput tool for investigating bone diagenesis: FTIR in attenuated total reflection (ATR) mode. Archaeometry 55, 507-532.

Hollund, H.I., Jans, M.M.E., Collins, M.J., Kars, H., Joosten, I., Kars, S.M., 2012. What happened Here? Bone histology as a tool in decoding the postmortem histories of archaeological bone from Castricum, The Netherlands. Int. J. Osteoarchaeol. 22, 537-548.

Holmes, J.M., Beebe, R.A., Posner, A.S., Harper, R.A., 1970, Surface areas of synthetic calcium phosphates and bone mineral. Proc. Soc. Exp. Biol. 133, 1250-1253.

Holmes, J.M., Davies, D.M., Meath, W.J., Beebe, R.A., 1964. Gas adsorption and surface structure of bone mineral. Biochemistry 3, 2019–2024.

Huisman, H., Ismail-Meyer, K., Sageidet, B.M., Joosten, I., 2017. Micromorphological indicators for degradation processes in archaeological bone from temperate European wetland sites. J. Archaeol. Sci. 85, 13-29.

Immel, A., Le Cabec, A., Bonazzi, M., Herbig, A., Temming, H., Schuenemann, V.J., Bos, K.I., Langbein, F., Harvati, K., Bridault, A., Poin, G., Julien, M.-A., Krotova, O., Conard, N.J., Münzen, S.C., Drucker, D.G., Voila, B., Hublin, J.-J., Tafforeau, P., Krause, J., 2016. Effect of X-ray irradiation on ancient DNA in sub-fossil bones – Guidelines for safe X-ray imaging. Sci. Rep. 6, 32969.

Jackes, M., Sherburne, R., Lubell, D., Barker, C., Wayman, M., 2001. Destruction of the microstructure in archaeological bone: a case study from Portugal. Int. J. Osteoarchaeol. 11, 415-432.

Jacob, E., Querci, D., Caparros, M., Barroso Ruiz, C., Higham, T., Deviése, T., 2018. Nitrogen content variation in archaeological bone and its implications for stable isotope analysis and radiocarbon dating. J. Archaeol. Sci. 93, 68-73.

Jans, M.M.E., Kars, H., Nielsen-Marsh, C.M., Smith, C.I., Nord, A.G., Arthur, P., Earl, N., 2002. In situ preservation of archaeological bone. A histological study within a multidisciplinary approach. Archaeometry 44, 343-352.

Jans, M.M.E., Nielsen-Marsh, C.M., Smith, C.I., Collins, M.J., Kars, H., 2004. Characterisation of microbial attack on archaeological bone. J. Archaeol. Sci. 33, 87-95.

King, C.L., Tayles, N., Gordon, K.C., 2011. Re-examining the chemical evaluation of diagenesis in human bone apatite. J. Archaeol. Sci. 38, 2222-2230.

Kottler, C., Döbeli, M., Krähenbühl, U., Nussbaumer, M., 2002. Exposure age dating by fluorine diffusion. Nucl. Instr. Meth. Phys. Res. B 188, 61-66.

Le Garff, E., Mesli, V., Delannoy, Y., Colard, T., Demondion, X., Becart, Anne, Hedouin, V., 2017. Technical note: early post-mortem changes of human bone in taphonomy with μCT. Int. J. Legal Med. 131, 761-770.

Lebon, M., Reiche, I., Gallet, X., Bellot-Gurlet, L., Zazzo, A., 2016. Rapid quantification of bone collagen content by ATR-FTIR spectroscopy. Radiocarbon 58, 131–45.

Lebon, M., Zazzo, A., Reiche, I., 2014. Screening in situ bone and teeth preservation by ATR-FTIR mapping. Palaeogeogr. Palaeoclimatol. Palaeoecol. 416, 110-119.

Lees, S., 1989. Some characteristics of mineralized collagen. In Hukins, D.W. (ed.) Calcified Tissue: Topics in Molecular and Structural Biology. London: Macmillan, pp. 153-173.

Lloyd, S.A.J., Bandstra, E.R., Travis, N.D., Nelson, G.A., Bourland, J.D., Pecaut, M.J., Gridley, D.S., Willey, J.S., Bateman, T.A., 2008. Spaceflight-relevant types of ionizing radiation and cortical bone: Potential LET effect? Adv. Space Res. 42, 1889-1897.

Lowell, S., Shields, J.E., Thomas, M.A., Thommes, M., 2004. Characterization of Porous Solids and Powders: Surface Area, Pore Size, and Density, Springer Netherlands, ISBN 978-1-4020-2302-6.

Lowenstein, H. A,, and Weiner, S., 1989. On Biomineralization, Oxford University Press, Oxford, p. 151.

Madden, O., Chan, D.M.W., Dundon, M., France, C.A.M., 2018. Quantifying collagen quality in archaeological bone: Improving data accuracy with benchtop and handheld Raman spectrometers. J. Archaeol. Sci. Rep. 18, 596-605.

Marchiafava, V., Bonucci, E., Ascenzi, A., 1974. Fungal osteoclasia: a model of dead bone resorption. Calc. Tissue Res. 14, 195–210.

Misra, D.N., Bowen, R.L., Mattamal, G.J., 1978. Surface area of dental enamel, bone, and hydroxyapatite: Chemisorption from solution. Calcif. Tissue Res. 26, 139-142.

Morris, M.D., Finney, W.F., 2004. Recent developments in Raman and infrared spectroscopy and imaging of bone tissue. Spectroscopy 18, 155-159.

Muller, H.J., 1927. Artificial transmutation of the gene. Science 66, 84-97.

Ngan-Tillard, D.J.M., Huisman, D.J., 2017, Micro-CT Scanning. In: Nicosia, C., Stoops, G. (eds) Archaeological Soil and Sediment Micromorophology, Wiley Blackwell, Chichester, Sussex, pp. 441-449.

Nielsen-Marsh, C.M., Hedges, R.E.M., 1999. Bone porosity and the use of mercury intrusion porosimetry in bone diagenesis studies. Archaeometry 41, 165-174.

Nielsen-Marsh, C.M., Hedges, R.E.M., 2000. Patterns of diagenesis in bone I: the effects of site environments. J. Archaeol. Sci. 27, 1139-1150.

Nielsen-Marsh, C.M., Hedges, R.E.M., Mann, T., Collins, M.J., 2000. A preliminary investigation of the application of Differential Scanning Calorimetry to the study of collagen degradation in archaeological bone. Thermochim. Acta 365, 129-139.

Nielsen-Marsh, C.M., Smith, C.I., Jans, M.M.E., Nord, A., Kars, H., Collins, M.J., 2007. Bone diagenesis in the European Holocene II: taphonomic and environmental considerations. J. Archaeol. Sci. 34, 1523-1531.

Paredes, U.M., Prys-Jones, R., Adams, M., Groombridge, J., Kundu, S., Agapow, P.-M., Abel, R.L., 2012. MicroCT X-rays do not fragment DNA in preserved bird skins. J. Zool. Syst. Evol. Res. 50, 247-250.

Parker, R.B., Murphy, J.W., Toots, H., 1974. Fluorine in fossilized bone and tooth: Distribution among skeletal tissues. Archaeometry 16, 98-102.

Pestle, W.J., Ahmad, F., Vesper, B.J., Cordell, G.A., Colvard, M.D., 2014. Ancient bone collagen assessment by hand-held vibrational spectroscopy. J. Archaeol. Sci. 42, 381-389.

Pestle, W.J., Brennan, V., Sierra, R.L., Smith, E.K., Vesper, B.J., Cordell, G.A., Colvard, M.D., 2015. Hand-held Raman spectroscopy as a pre-screening tool for archaeological bone. J. Archaeol. Sci. 58, 113–20.

Reiche, I., Favre-Quattropani, L., Vignaud, C., Bocherens, H., Charlet, L., Menu, M., 2003. A multi-analytical study of bone diagenesis: the Neolithic site of Bercy (Paris, France). Meas. Sci. Technol. 14, 1608-1619.

Rusak, D.A., Marisco, R.M., Taroli, B.L., 2011, Using Laser-Induced Breakdown Spectroscopy to Assess Preservation Quality of Archaeological Bones by Measurement of Calcium-to-Fluorine Ratios. Appl. Spect. 65, 1193-1196.

Sealy, J., Johnson, M., Richards, M., Nehlich, O., 2014. Comparison of two methods of extracting bone collagen for stable carbon and nitrogen isotope analysis: comparing whole bone demineralization with gelatinization and ultrafiltration. J. Archaeol. Sci. 47, 64-69.

Smith, C.I., Nielsen-Marsh, C.M., Jans, M.M.E., Arthur, P., Nord, A.G., Collins, M.J., 2002. The strange case of Apigliano: Early 'fossilization' of Medieval bone in southern Italy. Archaeometry 44, 405-415.

Smith, C.I., Nielsen-Marsh, C.M., Jans, M.M.E., Collins, M.J., 2007. Bone diagenesis in the European Holocene I: patterns and mechanisms. J. Archaeol. Sci. 234, 1485-1493.

Sołtysiak, A., Miśta-Jakubowska, E.A., Dorosz, M., Kosiński, T., Fijał-Kirejczyk, I., 2018. Estimation of collagen presence in dry bone using combined X-ray and neutron radiography. Appl. Radiat. Isot. 139, 141-145.

Stathopoulou, E.T., Psycharis, V., Chryssikos, G.D., Gionis, V., Theodorou, G., 2008. Bone diagenesis: New data from infrared spectroscopy and X-ray diffraction. Palaeogeogr. Palaeoclimatol. Palaeoecol. 266, 168-174.

Surovell, T.A., Stiner, M.C., 2001. Standardizing infra-red measures of bone mineral crystallinity: an experimental approach. J. Archaeol. Sci. 28, 633-642..

Tripp, J.A., Squire, M.E., Hamilton, J., Hedges, R.E.M., 2010. A nondestructive prescreening method for bone collagen content using micro-computed tomography. Radiocarbon 52, 612-619.

Trueman, C.N., Martill, D.M., 2002. The long-term survival of bone: the role of bioerosion. Archaeometry 44, 371-382.

Trueman, C.N., Privat, K.L., Field, J., 2008. Why do crystallinity values fail to predict the extent of diagenetic alteration of bone mineral? Palaeogeogr. Palaeoclimatol. Palaeoecol. 266, 160-167.

Tuniz, C., Zanini, F., 2014. Microcomputerized Tomography (MicroCT) in Archaeology. In: Smith, C. (ed) Encyclopedia of Global Archaeology. Springer, New York, NY, pp. 4878-4884.

Turner-Walker, G., Nielsen-Marsh, C.M., Syversen, U., Kars, H., Collins, M.J., 2002. Sub-micron spongiform porosity is the major ultra-structural alteration occurring in archaeological bone. Int. J. Osteoarchaeol. 12, 407-414.

Turner-Walker, G., Parry, T.V., 1995. The Tensile Strength of Archaeological Bone. J. Archaeol. Sci. 22, 185-191.

Turner-Walker, G., Syversen, U., 2002. Quantifying histological changes in archaeological bones using BSE-SEM image analysis. Archaeometry 44, 461–8.

Van Klinken, G. J., 1999. Bone collagen quality indicators for palaeodietary and radiocarbon measurements. J. Archaeol. Sci. 26, 687–95.

Webb, P.A., Data Collection, Reduction and Presentation, Micromeritics Sales Support Document, April 1993.

Weiner, S., Price, P.A., 1986. Disaggregation of bone into crystals. Calcif. Tissue Res. 39, 365-375.

Wolff, S., 1971. Radiation genetics. Annu. Rev. Genet. 1, 221-244.

Wood, N.V., 1947, Specific surfaces of bone, apatite, enamel and dentine. Science 105, 531-532.

Wright, L.E., Schwarcz, H.P., 1996. Infrared and isotopic evidence for diagenesis of bone apatite at dos Pilas, Guatemala: palaeodietary implications. J. Archaeol. Sci. 23, 933-944.

Yoshino, M., Kimijima, T., Miyasaka, S., Sato, H., Seta, S., 1991. Microscopic study on estimation of time since death in skeletal remains. Forensic Sci. Int. 49, 143-158.

Table 1. Terms for pore size ranges used in this report (after Turner-Walker, et al. 2002)

Term	Pore size	Features in size range
Micropore	<0.1 μm	Space left by collagen fibril degradation
Mesopore	0.1-1 μm	Normal physiological features such as canaliculi, and channels resulting from bacterial degradation
Macropore	>1 μm	Normal physiological features such as Haversion canals, fungal (Wedl) tunneling, and space left after mineral dissolution

Table 2. List of bones used in this study along with essential measured parameters.

Sample number	% collagen[a]	C:N ratio of collagen[b]	Ct.Po[c]	Porosity (%)[d]	Surface area (m^2/g)[e]	Ca/F ratio[f]
Cattle Bones						
ET2	1.1	3.3	0.0350		119.6	7.58
ET4	9.7	3.2	0.0027			7.71
ET8	6.5	3.2	0.3045			
ET10	0	-	0.1429			
ET12	5.7	3.3	0.7596			8.47
ET16	0	-	0.4890			2.12
ET18	0	-	0.4448			1.45
ET20	6.5	3.3	0.1207			8.38
ET22	0	-	0.6148			
Sheep Bones						
ET46	13.4	3.3	0.0060	13.45	68.9	6.44
ET47	17.0	3.3	0.0007			5.70
ET49	0	-	0.5787			3.86
ET50	0	-	0.3315		104.4	4.44
ET51	0	-	0.7852	50.02	121.3	2.92
ET53	0	-	0.0491			
ET54	0	-	0.0904			
ET55	0	-	0.0027			
ET60	0	-	0.0096	37.37	127.5	5.64
ET62	3.0	3.4	0.1262	30.57	82.8	5.72

[a] % collagen is calculated by dividing the mass of recovered collagen by the mass of bone used for the extraction. Details of the collagen extraction procedure are provided in Hamilton & Hedges 2011, where these values were first published.

[b] C:N ratios were measured by IRMS and reported in Hamilton & Hedges 2011.

[c] Ct.Po is calculated from microCT images using the method discussed in this paper and Tripp, et al. 2010, using cylindrical contours and threshold=500.

[d] Total bulk porosity as measured by HgIP.

[e] Surface area as measured by BET nitrogen adsorption.

[f] Ca 671.8 / F 685.6 ratio measured by LIBS, average of ten pulses beginning with pulse 210. Details of the experimental methods and results are reported in Rusak, et al. (2011).

Figure 1. Microcomputed tomography (microCT) images of five of the bones used in this study. (A) ET18 (top) and ET12 (bottom), (B) ET60 (top, two pieces), ET62 (bottom left, three pieces), and ET51 (bottom right). Additional images of bones from the assemblage appear in Tripp, et al. 2010.

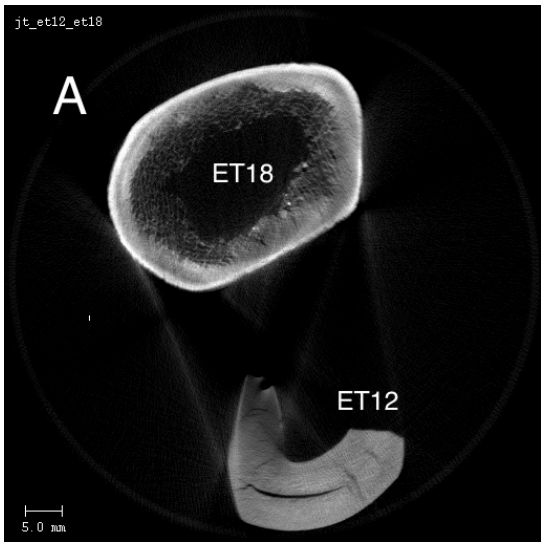

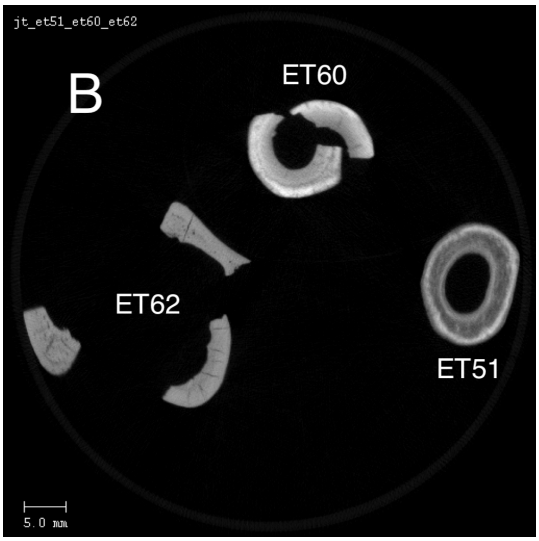

Figure 2. Contour images from bones calculated from microCT measurements at a threshold of 500. Images for all bones can be viewed in Supplemental Information.

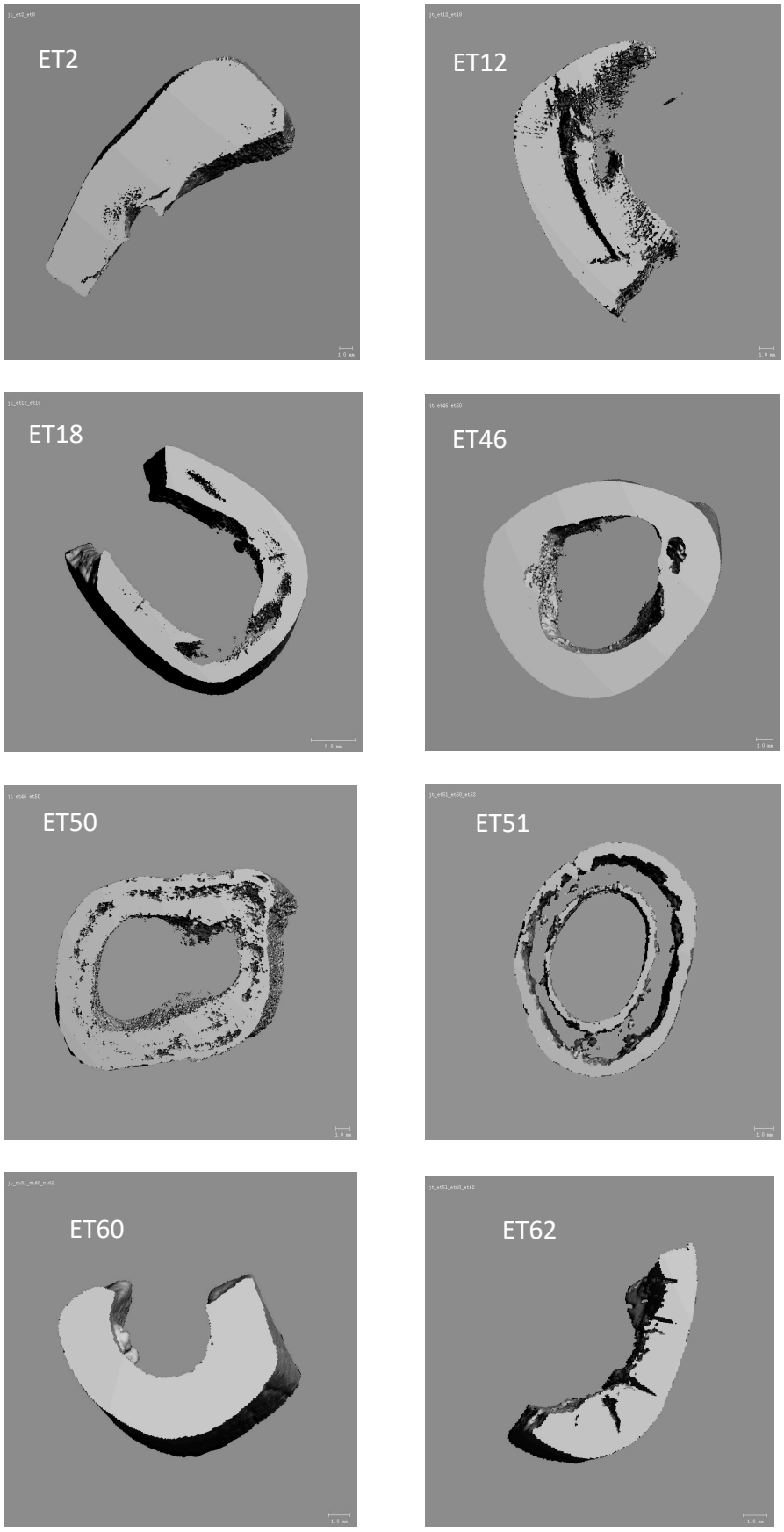

Figure 3. Cortical porosity calculated from microCT, correlated with % collagen recovery from 19 Etton sheep and cattle bones. ☐ represents samples with no collagen preservation, ● denotes samples with useful amount (>1% by mass) of recovered collagen.

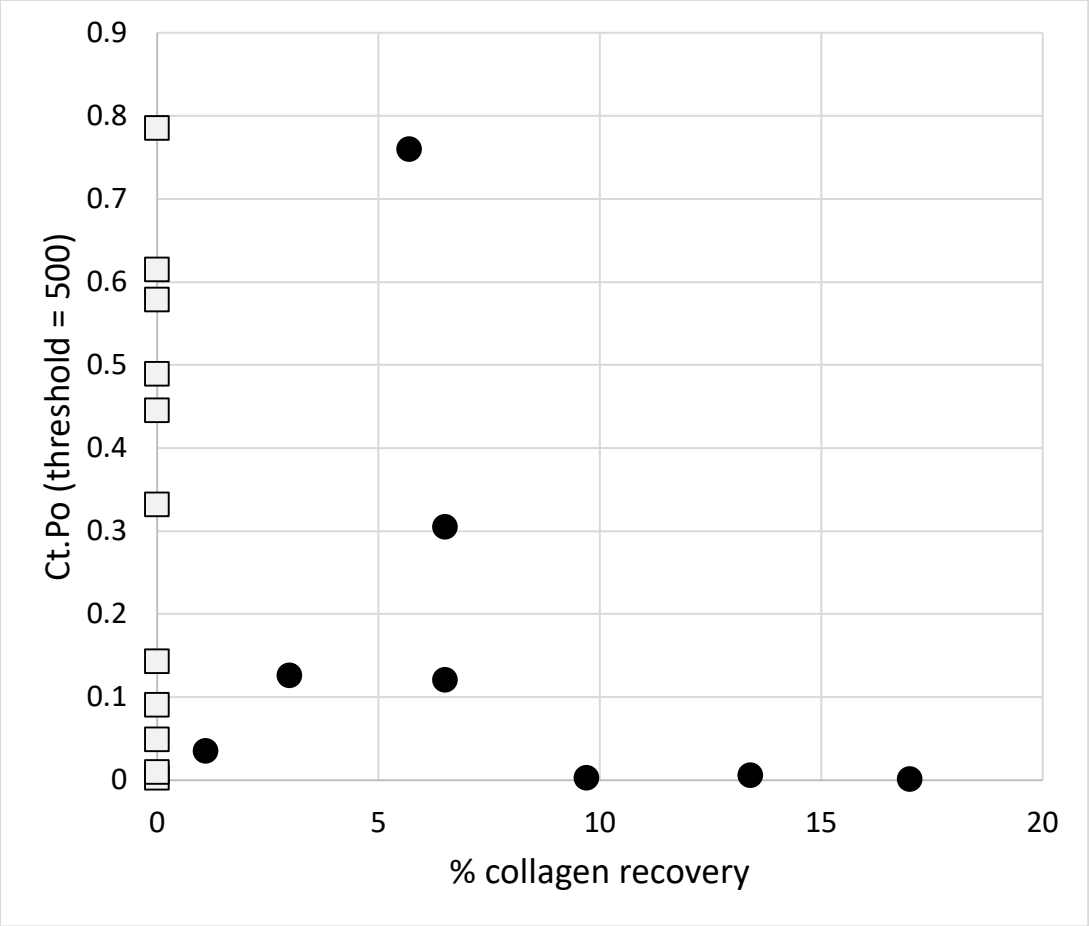

Figure 4. Differential pore size distributions, measured by HgIP, for fresh modern bone (dark line) and modern bone that was deproteinated using hydrazine (light line). Figure was produced using data from Nielsen-Marsh and Hedges 1999 (with permission from R. Hedges), and experimental details for deproteination can also be found therein.

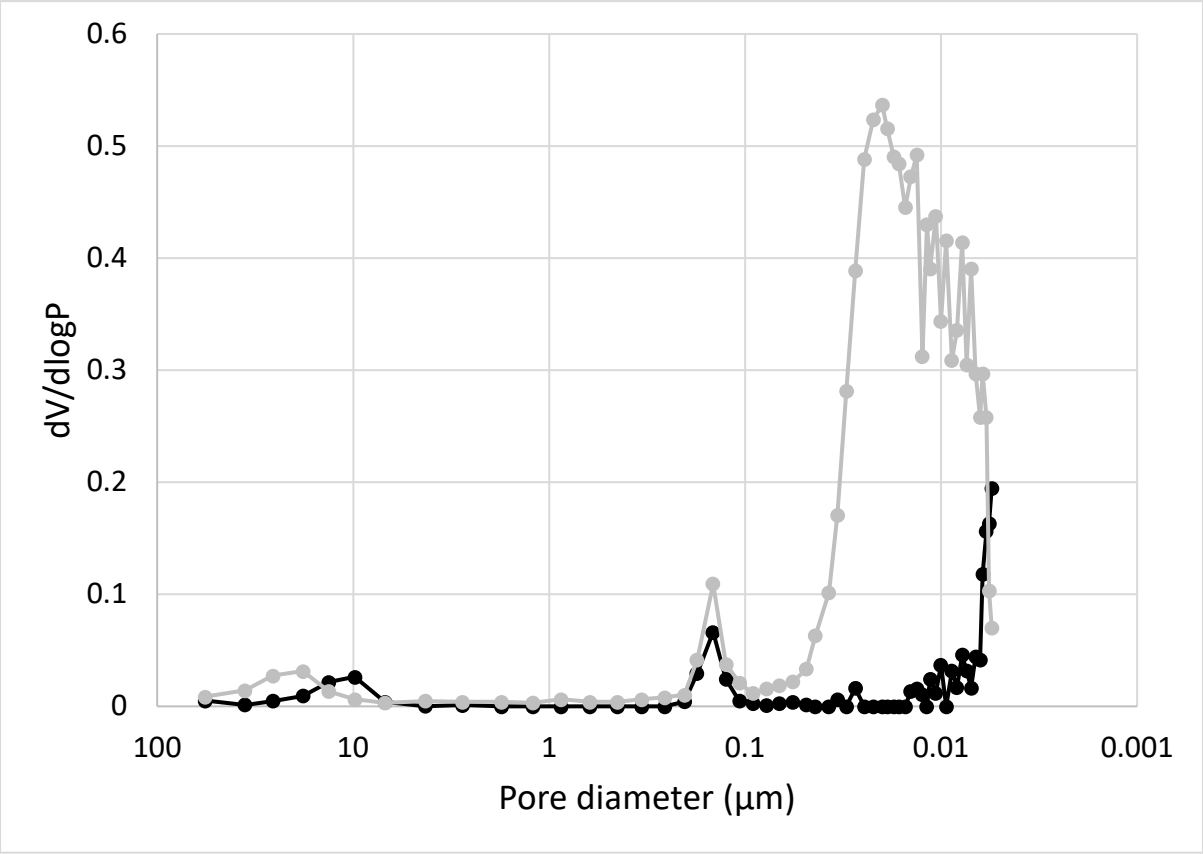

Figure 5. Pore size distributions measured by HgIP for four Etton sheep bones: ET46 (black solid line, 13.4% collagen), ET51 (gray solid line, 0% collagen), ET60 (gray dotted line, 0% collagen), and ET62 (black dashed line, 3.0% collagen).

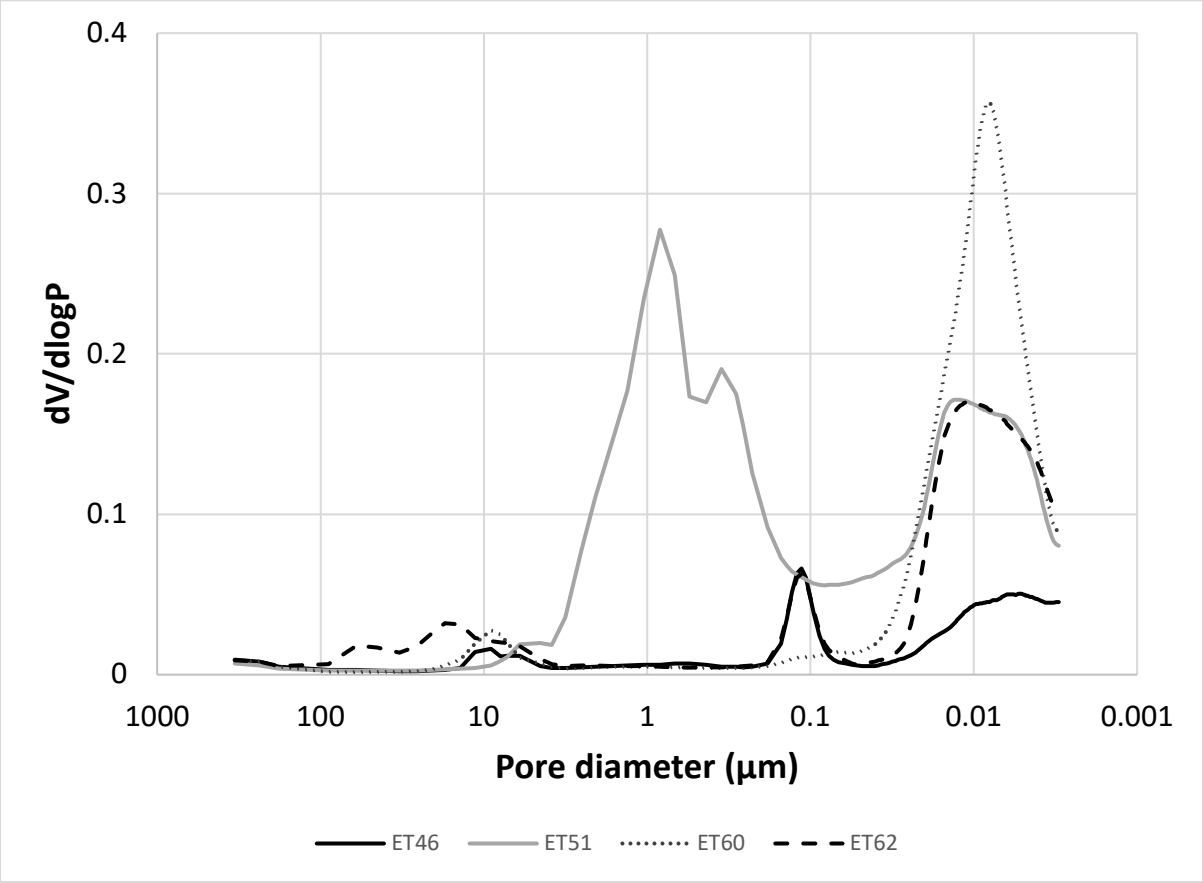

Figure 6. Percent collagen recovery from six bones correlated with surface area as measured by BET nitrogen adsorption (▲, left axis) and cortical porosity as calculated from microCT (●, right axis).

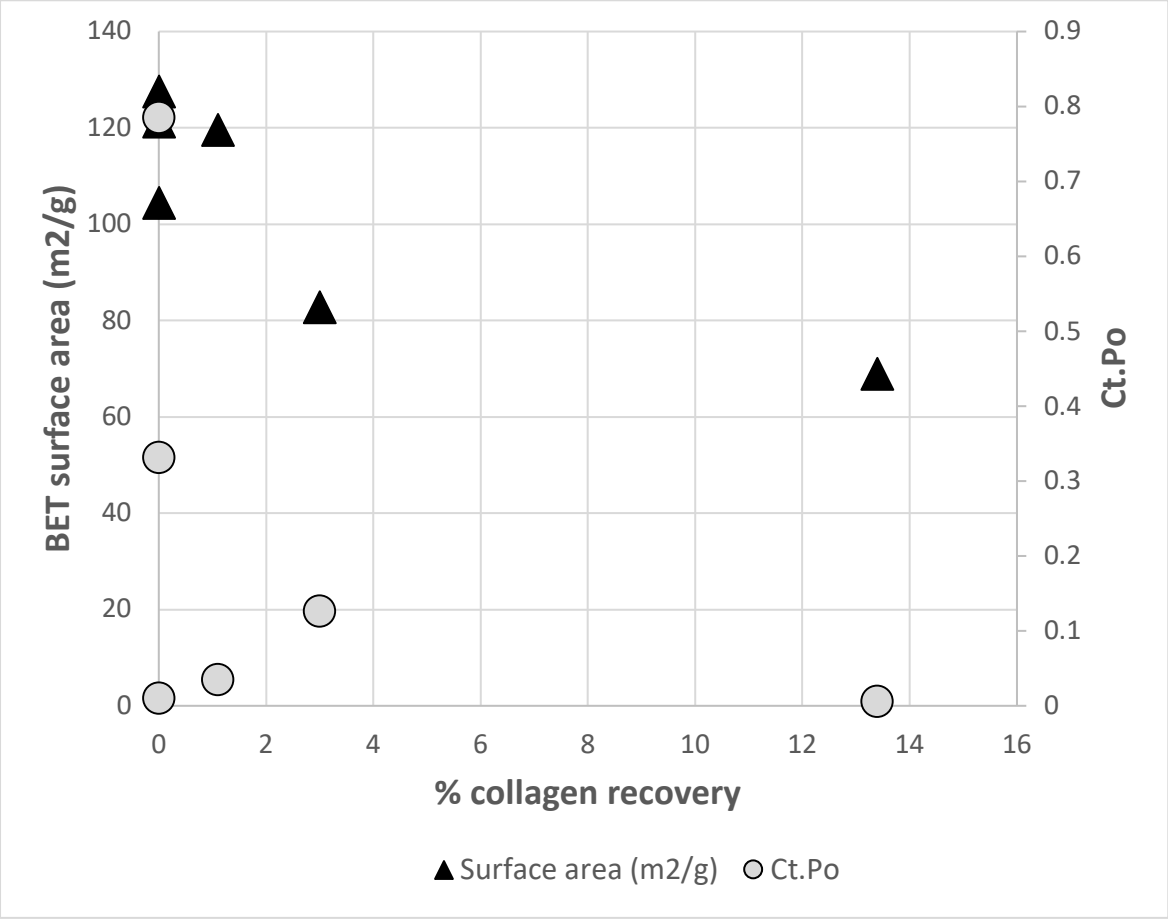

Figure 7. Ca/F ratio from thirteen Etton bones analyzed by LIBS. Experimental details and measurements used to make the graph were first published by Rusak, et al. (2011, Table II). Bones with no collagen recovery (black lines) have a lower Ca/F ratio than those with higher collagen recovery (gray lines), after the initial laser pulses.

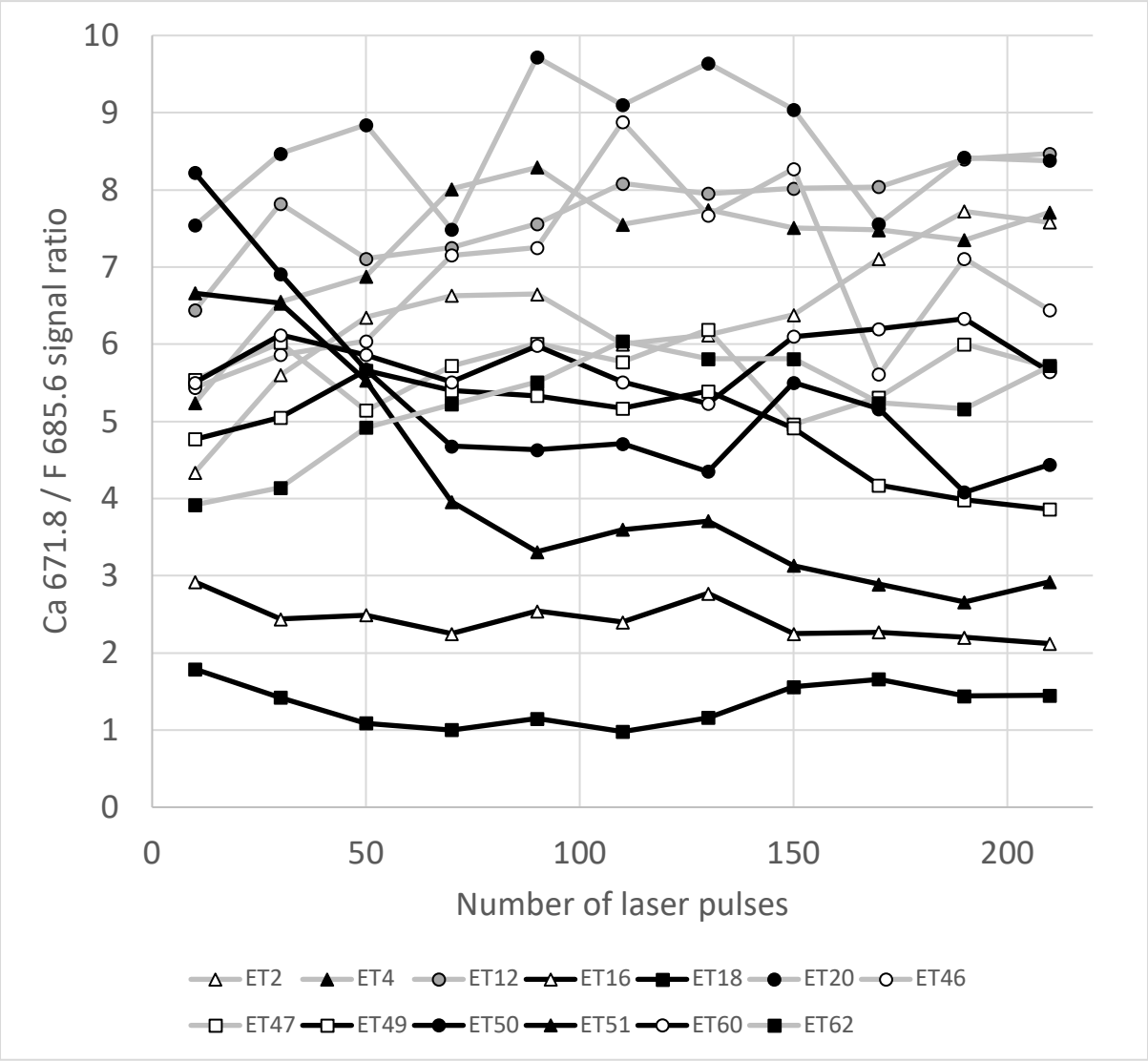

Figure 8. Average Ca/F ratios for bones measured by LIBS. Average and standard deviation for bones with no collagen preservation (black dots, N=7), and bones with >1% collagen extracted (gray dots, N=6). Calculations use data from Rusak, et al. (2011, Table II).

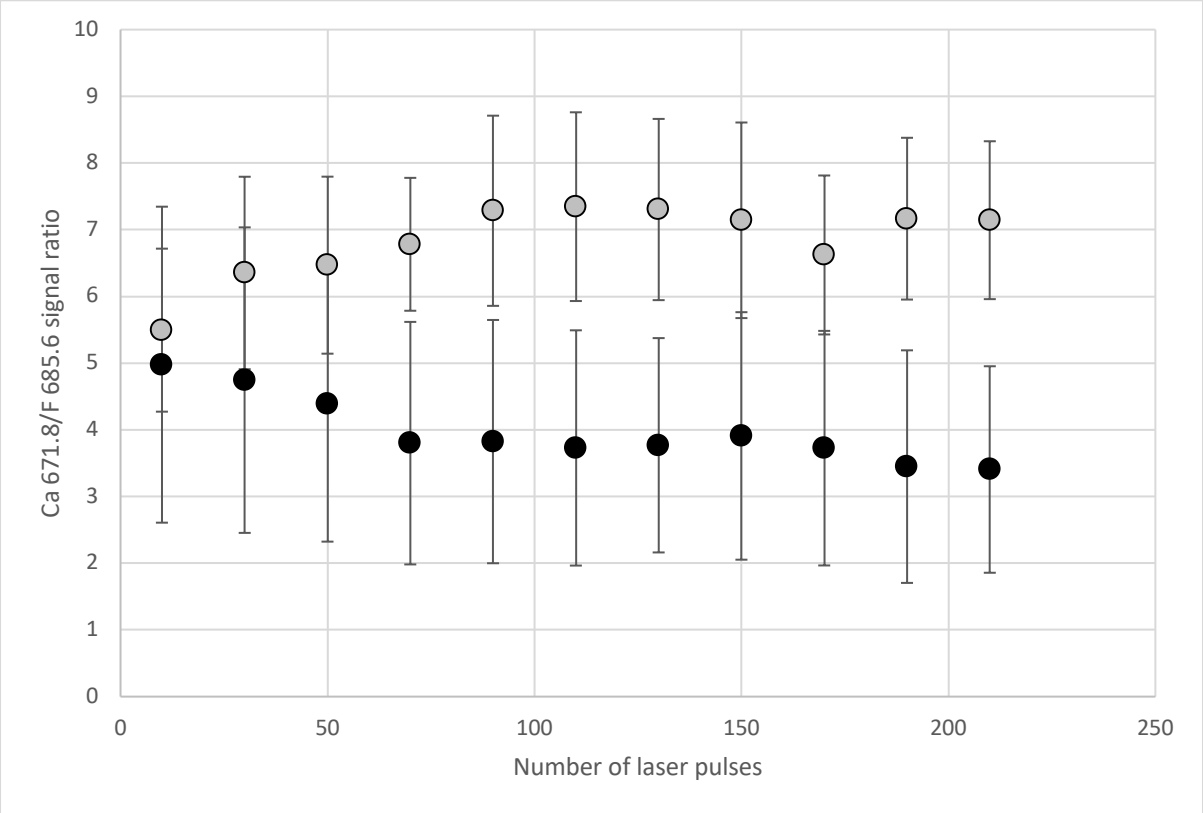

Supplementary information
Calculated 3-D contour images for Etton bones.

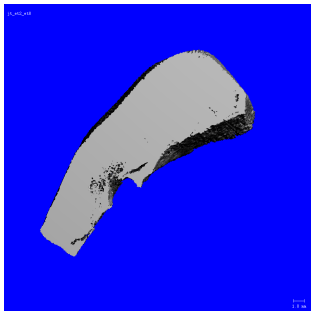
ET2

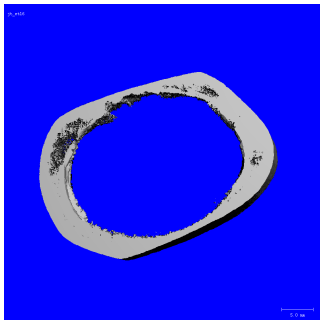
ET16

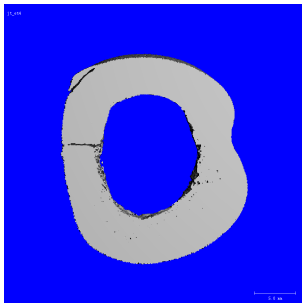
ET4

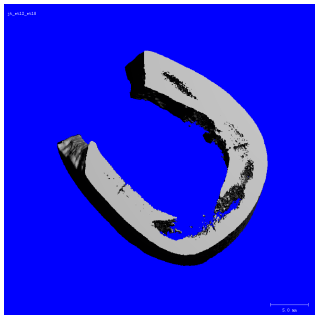
ET18

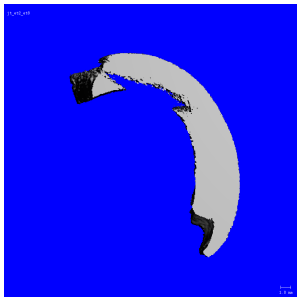
ET8

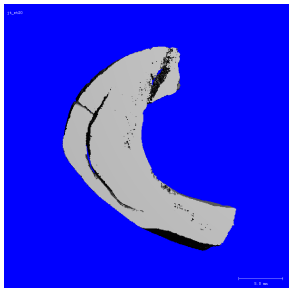
ET20 – fragment 1


ET10

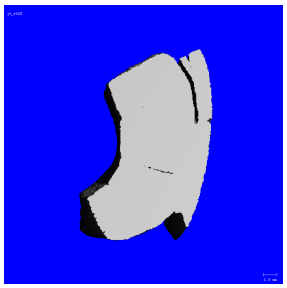
ET20 – fragment 2

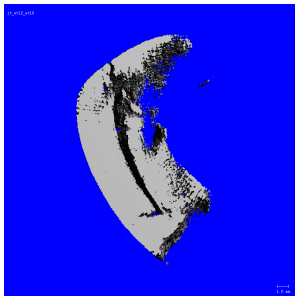
ET12

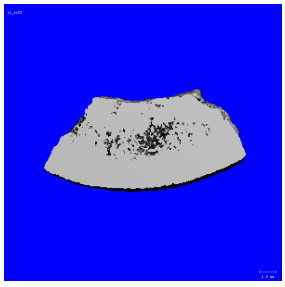
ET20 – fragment 3

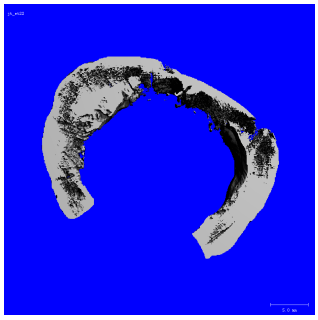

ET22

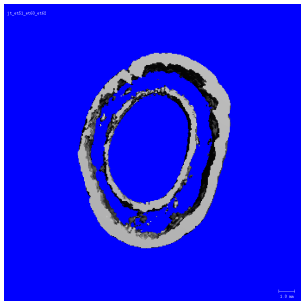

ET51

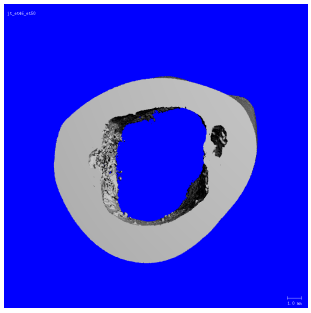

ET46

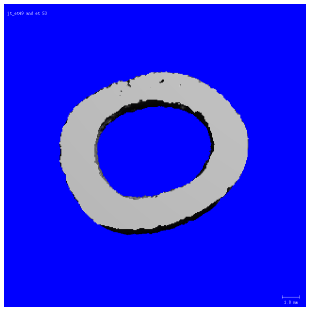

ET53

ET47

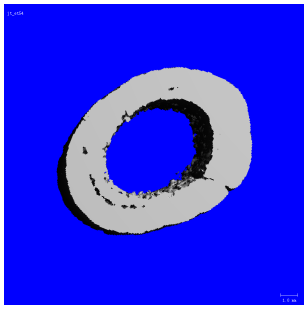

ET54

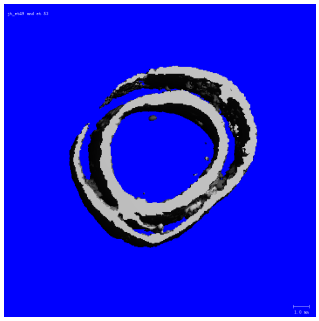

ET49

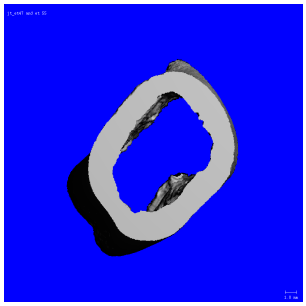

ET55

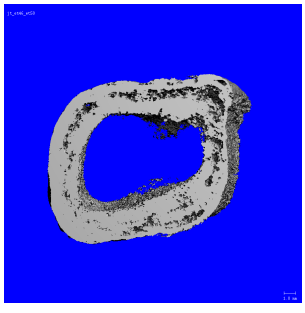

ET50

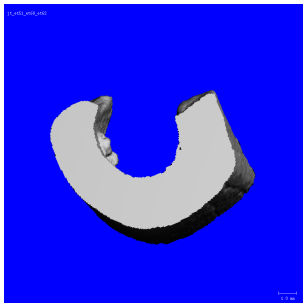

ET60 – fragment 1

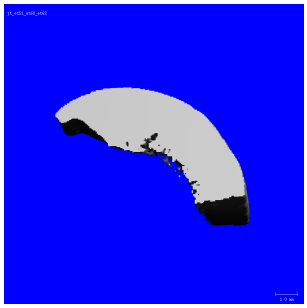
ET60 – fragment 2

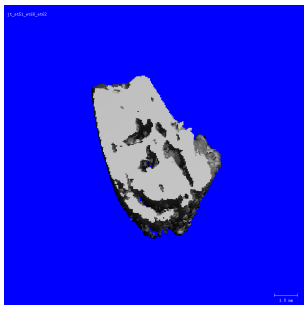
ET62 – fragment 1


ET62 – fragment 2


ET62 – fragment 3